Bottom–up propagation of synoptic wind intensification and relaxation in the planktonic ecosystem of the South Senegalese Upwelling Sector

Pierre Chabert, Vincent Echevin, Olivier Aumont, Renaud Person, Christophe Hourdin, Stéphane Pous, Éric Machu, Xavier Capet

Bottom-up propagation of synoptic wind intensification and relaxation in the planktonic ecosystem of the South Senegalese Upwelling Sector

P. Chabert[1], V. Echevin[1], O. Aumont[1], R. Person[2], C. Hourdin[1], S. Pous[1], E. Machu[3], X. Capet[1]

[1]Sorbonne Université, CNRS, IRD, MNHN, Laboratoire d'Oceanographie et du Climat: experimentations et Approches Numeriques (LOCEAN-IPSL), Paris, France; [2]Sorbonne Université, CNRS, IRD, MNHN, OSU Ecce Terra, LOCEAN-IPSL, Paris, France; [3]Université de Bretagne Occidentale, CNRS, IRD, Ifremer, Laboratoire d'Océanographie Physique et Spatiale (LOPS), IUEM, Brest, France
Corresponding author: pierre.chabert@locean.ipsl.fr

Abstract

Synoptic intensification or relaxation of upwelling favorable winds are major sources of variability in Eastern Boundary Upwelling systems. This study aims to investigate their impact on the planktonic ecosystem of the South Senegalese Upwelling Sector (SSUS), located south of the Cape Verde peninsula over a wide and shallow continental shelf. Numerical experiments using a three dimensional coupled physical-biogeochemical model with four plankton functional types simulated the response of the coastal planktonic ecosystem to idealized synoptic (~10 days) wind intensification and relaxation of the same amplitude. We find that these perturbations induce spatio-temporal oscillations of plankton concentrations. Zooplankton response occurred with a time lag that manifests itself in space as an equatorward/downstream shift in distribution relative to phytoplankton. Overall, the transmission of the synoptic perturbation from the physics to zooplankton is characterised by a damping in relative anomalies. All these elements and the weakness of the asymmetries in the biogeochemical/planktonic ecosystem responses between intensification and relaxation events support the hypothesis that synoptic variability has limited impact on the climatological state of low-latitude upwelling systems such as the SSUS.

Plain Language Summary

In some coastal regions of the world such as off Senegal, winds preferentially blow alongshore and induce subsurface, cold and nutrient rich waters to rise to the surface layer and favor the development of plankton blooms. These so-called upwelling favorable winds are not steady. Their fluctuations produce dynamical and biogeochemical variability over a broad range of scales. Here we studied the biogeochemical effect of 10-day (i.e. weather or synoptic) wind fluctuations over the southern Senegal continental shelf. We used a numerical model with a simplified planktonic ecosystem consisting of two phytoplankton and two zooplankton size classes. The wind perturbations modulate ocean physics, the enrichment of the sun-lit surface layer in nutrients and the planktonic ecosystem. The plankton's response to wind fluctuations exhibited oscillations more complex and relatively less intense than those of the wind. The modest effect of the studied short-term wind fluctuations on plankton found in this study may be specific to low-latitude coastal oceans with wide continental shelves.

1 Introduction

Alongshore upwelling favorable winds provide eastern boundary upwelling systems with nutrient and plankton rich surface waters, with great implications for the local and global fishing activities (Fréon et al., 2009; Chavez & Messié, 2009). In addition to their seasonality and low frequency variability, these winds fluctuate on synoptic (3-10 days) and intraseasonal (< 2 months) time scales. This fluctuation affects the physics, carbon cycling, as well as the ecosystem dynamics of coastal upwellings (Largier et al., 2006; Spitz et al., 2005; Desbiolles et al., 2014; Capet et al., 2017; Galán et al., 2020; Aguirre et al., 2021). In our domain of interest offshore of West Africa the shorter synoptic time scale tends to dominate over longer ones (Tall et al., 2021). We will thus restrict our attention to this range of scales. Synoptic variability consists of a succession of intensifications and relaxations of upwelling favorable winds. Associated modulations of the Ekman transport and wind stress curl (hence also of Ekman pumping and lateral Sverdrup transport), and of mixing rates and stratification (Largier et al., 2006; Jacox & Edwards, 2011) are the most common ways physics affect marine primary production and food webs. Previous studies have uncovered situations in which synoptic wind variability produced flow disturbances that have plausibly large implications on plankton dynamics and the reproductive strategies of many marine animals (Botsford et al., 2003, 2006).

The effect of synoptic variability on primary production, and more generally on the functioning of

upwelling ecosystems is not well understood. (Largier et al., 2006) and (Wilkerson et al., 2006) described the importance of sequences involving an upwelling wind intensification (inducing a pulse of nutrients in the euphotic layer) followed by a wind relaxation (leading to restratification and a plankton bloom). In the idealized 2D vertical setting of Botsford (Botsford et al., 2006) synoptic variability could be beneficial or detrimental to bulk primary/secondary production of a continental shelf. In an upwelling sector where average winds are high and/or the shelf is narrow wind relaxation periods allowed for an intermittently better utilization of upwelled nutrients. Conversely, in a system where average winds are low and/or the shelf is relatively wide, strong episodic upwelling events generally accelerated offshore export and/or subduction of upwelled nutrients (Evans et al., 2015) which may not have been converted into plankton biomass. This conceptual landscape is broadly consistent with the evidence of optimal wind windows for primary production and plankton stock (Yokomizo et al., 2010; Jacox et al., 2016). Beside shelf width and wind regime, the oceanic response to synoptic variability depends on the specificities of each upwelling sector. These specificities include coastline geomorphological irregularities which exert important constraints on the flow (Largier, 2020; Spitz et al., 2005), (sub)mesoscale turbulence regime which can have a leading order effect on premature subduction of upwelled nutrients (Gruber et al., 2011; Renault et al., 2016; Hauschildt et al., 2021; Nagai et al., 2015), nearshore productivity and biomass/carbon export (Stukel et al., 2017; Chabert et al., 2021).

The continental shelf on which we focus, the southern Senegalese upwelling sector (SSUS), extends over approximately 5 degrees of latitude south of Dakar. Among its prime characteristics are a sharp coastline discontinuity toward its northern edge, a wide continental shelf further south (see Fig. 1), and low-to-moderate upwelling winds.

All this plays in favor of long retention time scales in comparison to other areas subjected to upwelling dynamics (Ndoye et al., 2017). Based on a qualitative application of Botsford's reasoning (Botsford et al., 2006), synoptic variability could strengthen offshore export during wind intensifications, leading to an overall deterioration of the retentive properties of the system. In more quantitative terms though, it is unclear if the acceleration of the upwelling flow during typical upwelling wind events can be sufficient to produce retention changes with a significant impact on coastal primary and secondary production.

In this study, our objective is to gain insight into the effect of synoptic variability of atmospheric forcings on the SSUS plankton dynamics. Specifically, we describe the cascade of the synoptic perturbation from physics to zooplankton (*e.g.*, the existence of damping or amplification between trophic levels), and characterise the asymmetries between the response to upwelling relaxation and intensification events (as

previously done for ocean physics, see (Chabert et al., 2023)). Quantifying asymmetric behaviours provides useful indications on the degree to which net rectification effects of synoptic variability (i.e., compensations between wind intensification and relaxation responses accounted for) impact the mean state and functioning of the real ocean (more details are given in section 2.5).

To do so we carried out 3D physics-biogeochemistry model experiments. The plankton ecosystem consisted of two phytoplankton and two zooplankton types. One deliberate model simplification concerned the synoptic fluctuations of the atmospheric forcing which were constructed so as to ensure perfect symmetry between wind intensification and relaxations events, thereby facilitating the identification of sources of asymmetry internal to the ocean. Having chosen to explore the effect of synoptic fluctuations of rather extreme magnitude, we found substantial plankton responses to them with biomass changes of ±20-50%. However there was an overall attenuation of the synoptic disturbances as they propagated from physics to zooplankton and also a relatively low degree of asymmetry between the responses, hence our general conclusion on the limited role played by synoptic variability in the SSUS.

Section 2 presents the methods and section 3 the model mean state (evaluation of the model using observations is shown in the supplementary material). The model response to symmetric atmospheric forcing anomalies is examined in sections 4 and 5. We describe in sequence: the domain-wide temporal evolution of the response during and after the synoptic fluctuations (section 4a); the disturbances of the spatial patterns produced within the SSUS (section 4b); and the bottom-up propagation of the synoptic anomalies (section 5). A discussion and some concluding remarks are given in section 6.

2 Modelling framework and methods

The framework described below was designed with the following specifications in mind: to preserve the degree of realism achieved by the configuration/setup used in (Ndoye et al., 2017); to add synoptic perturbations of the wind and net heat flux forcings representative of major upwelling intensification and relaxation events; to transition smoothly from climatological to synoptic forcing; to be able to identify the forced ocean response despite the turbulent nature of its dynamics. The former specification led us to use distinct atmospheric products for the climatological and synoptic anomaly components of the forcing. The latter motivated the computation of ensemble runs.

2.1 Physical and biogeochemical models

We developed a modelling framework based on an ensemble of perturbed coupled physical-biogeochemical simulations forced by an idealized synoptic forcing. Analysing the ensemble mean and spread reduced the effect of intrinsic variability permitting identification of the robust components of the synoptic responses. To model the ocean dynamics, we used the Coastal and Regional Ocean COmmunity model (CROCO, from `https://www.croco-ocean.org/`; Hilt et al. (2020)), derived from Regional Ocean Modeling System (ROMS; Shchepetkin and McWilliams (2005, 2009)). CROCO solves the primitive equations for a free-surface ocean in an earth-centered rotating environment. Its high-order numerical schemes and terrain-following vertical coordinates allow for a realistic representation of the fine scale fronts and flows prevalent in coastal environments. The K-Profile Parameterization (KPP; Large et al. (1994)) was used as vertical mixing scheme.
CROCO was coupled to the marine biogeochemistry model Pelagic Interactions Scheme for Carbon and Ecosystem Studies (PISCES, from `https://www.pisces-community.org/`; Aumont et al. (2015)). The latter represents the main nutrients (nitrate, phosphate, silicate and iron) and has four size-structured living compartments: nanophytoplankton (NANO), microzooplankton (MICRO), diatoms (DIA) and mesozooplankton (MESO). The size range of the diatom group is typically 5-80 μm. The vertical distribution of solar heating in the water column is influenced by the three-dimensional phytoplankton chlorophyll concentration field inducing horizontally inhomogeneous biomass-dependent thermal heating (Echevin et al., 2021).
The model configuration was inherited from (Ndoye et al., 2017) and (Chabert et al., 2023): a parent grid (can11) covering the Canary current system [32°W-6°W,7°N-36°N] with a spatial resolution of ~10 km and a child grid (sen2) centered on the Senegalese sector [20°W-16°W,12°N-18°N] at ~2.5 km were coupled using AGRIF two-way nesting (Debreu & Blayo, 2008). Both model domains use the same vertical grid parameters and 50 levels.

2.2 Generation of an ensemble of initial states

A climatological simulation was performed. It was forced at the air-sea interface by monthly climatological surface heat and freshwater fluxes from the International Comprehensive Ocean Atmosphere Data Set (COADS; years 1854-1992; spatial resolution Δx = 0.5°; Worley et al. (2005)), monthly SST from the Moderate Resolution Imaging Spectroradiometer (MODIS; years 2002-2018; Δx = 5 km; NASA (2014)) for SST restoring (Barnier et al., 1995), and monthly wind stress from the

Scatterometer Climatology of Ocean Winds (SCOW; 1999-2009; $\Delta x = 0.25°$; Risien and Chelton (2008)). A monthly climatology (2000-2008 period) of the Simple Ocean Data Assimilation (SODA; Carton and Giese (2008)) was imposed at the open boundaries. Initial conditions for the physical variables were provided from a previous simulation having reached equilibrium (Ndoye et al., 2017). For biogeochemical initial and boundary conditions, the World Ocean Atlas (WOA) climatology for nitrate, phosphate, silicate and oxygen (Garcia et al., 2018), the Global Data Analysis Project (GLODAP) climatology for dissolved inorganic and organic carbon (Key et al., 2004) and the climatological dust deposition of Tegen and Fung (Tegen & Fung, 1994) were used.

This climatological simulation was run for 7 years and reached statistical equilibrium after 2 years (see Supplementary Fig. 1). For each of the last 5 years of climatological simulation, restart states corresponding to March 1st were stored to initialize the synoptic ensemble runs. The physical and biogeochemical variables in these initial states differ due to the intrinsic chaotic variability of the non-linear coupled model. Ensemble averaging over the 5-member ensemble run was systematically performed for all fields shown or discussed. A brief evaluation of key biogeochemical variables (surface chlorophyll-a and nitrate, averaged over the upwelling season (January-March) for the last 5 years of simulation) is presented in the supplementary material (Figs. 2-4) .

2.3 Idealized synoptic forcing

The idealized synoptic forcing is defined as follows. The forcing anomaly consists of a spatial pattern $\phi'_{SF}(x,y)$ multiplied by a temporal amplitude modulation $f(t)$. The anomaly was added to the climatological forcing ϕ_{clim} as defined in Eq. 1:

$$\phi_{SF^{\pm}}(x,y,t) = \phi_{clim}(x,y,t) \pm f(t) \times \phi'_{SF}(x,y) \tag{1}$$

with ϕ an atmospheric forcing variable (wind stress or air-sea net heat flux). $\phi'_{SF}(x,y)$ and $f(t)$ were built using ERA5 reanalyses (Hersbach et al., 2018). By construction the synoptic intensification and relaxation anomalies were symmetric. Having perfectly symmetric SF^{+} and SF^{-} forcings ensures that any asymmetry in the ocean state and functioning is produced by nonlinearities internal to the system. In nature or more realistic models, sources of asymmetry other than that considered are present, for instance when atmospheric forcings are represented with a bulk formula, as symmetric wind fluctuations would produce asymmetric wind stress and heat flux perturbations.

The amplitude of these anomalies was modulated in time ($f = f(t)$) over a 10-day window with a ramp

up, a plateau and a ramp-down back to 0 (see grey dashed line in Fig. 3a). The amplitude of the perturbation was determined using the distribution of 10-day averaged intraseasonal wind stress anomalies in ERA5 (see Table 1 for the wind and Fig. 2 in (Chabert et al., 2023)). The net air-sea heat flux perturbation was of the order of $\pm 30\ W.m^{-2}$, *i.e.*, comparable to the net flux itself at that season ($\sim$ 30-40 $W.m^{-2}$), but with limited spatial contrasts and therefore a modest dynamical impact (Chabert et al., 2023). Our wind anomalies ($\pm 0.032\ N.m^{-2}$) roughly belonged to the 95th percentile of the distribution (see Table 1). Although it may seem extreme, this choice is appropriate to produce a significant response of the ecosystem to the wind synoptic fluctuations.

The symmetric atmospheric perturbations, an upwelling favorable wind intensification (positive Synoptic Forcing perturbation: SF^+) and a relaxation (negative Synoptic Forcing perturbation: SF^-), were added to the climatological forcing and used to force the ensemble simulations, starting on 1 March (day 0 in our analysis). The reference simulations without perturbation (corresponding to the climatological simulation) are denoted SF^0. Additional information about how we ensured a smooth transition from climatological to synoptic forcings and how we dealt with net heat flux anomalies can be found in (Chabert et al., 2023).

2.4 Tracer tendency terms

To help interpret the synoptic evolution of the biogeochemical tracers of interest for our study (i.e. NO_3, NANO, DIA, MICRO, MESO), we used budget analyses in which tendency for any variable X was decomposed as:

$$\partial_t X = F_X^{Phy} + F_X^{Bio} \tag{2}$$

where F_X^{Phy} and F_X^{Bio} are respectively the lumped physical (advection and mixing) and biogeochemical tendency terms stored online during the model computation and output at daily frequency. Time series of these terms averaged over the shelf are analyzed in the following sections.

2.5 Synoptic response indicators

There have been frequent suggestions that (zero-mean) synoptic variability of atmospheric forcings could have an important effect on the mean state of upwelling systems (Send et al., 1987; Wilkerson et al., 2006; Iles et al., 2012). The simplest way this can happen is if the ocean responses to upwelling wind intensification and relaxation are not fully symmetric. This is precisely what our model framework

allowed us to investigate. To quantify the net residual/rectification effects due to synoptic variability of atmospheric forcings, we determined the degree of asymmetry of the $SF^{\pm}$ simulations relative to the climatological reference SF^0. This was done by computing a residual index defined as $\mathcal{R}_{SF}(X) = \frac{\frac{1}{2}(X_{SF^+} + X_{SF^-})}{X_{SF^0}} - 1$ for any model variable X. To account for the history of the synoptic responses, we present cumulative averages of $\mathcal{R}_{SF}$ (expressed in %) from the onset of the synoptic perturbation: $\mathcal{S}_{SF}(X,T) = \frac{1}{T}\int_0^T \mathcal{R}_{SF}(X)dt$. By construction, $\mathcal{S}_{SF}(X,T) \approx 0$ at T=30 days (i.e. the end of SF experiments when synoptic responses have faded away) would mean that a synoptic forcing combining an equal proportion of $SF^{\pm}$ events with no interplay between the events has a negligible net effect on X, relative to the magnitude of its climatological state.

We are also interested in comparing the magnitude of the ocean response to $SF^{\pm}$ for the different biogeochemical variables. To this end, we introduced $\mathcal{W}^{\pm 0}(X) = \overline{(\frac{X_{SF^{\pm}} - X_{SF^0}}{X_{SF^0}})}^{[t_1(X):t_2(X)]}$, which indicates the relative anomaly of X averaged over the 3-day interval $[t_1(X) : t_2(X)]$ chosen when variable X was most perturbed during the SF simulations (intervals are indicated for each variable in the upper part of each panel in Fig. 2). For each member i, the relative anomaly $\mathcal{W}_i^{\pm 0}$ is computed. The ensemble mean of this indicator is also plotted (see Fig. 5).

3 Physical and planktonic ecosystem mean states

The dynamics of the SSUS was strongly constrained by the geomorphology of the area. In short, robust spatial hydrological features existed during the upwelling season: i) a cold upwelling wake that originated south of the Cape Verde peninsula (~14.7°N) and approximately followed the 20-30 m isobath over a meridional distance of 100 km or more (Fig. 1a,d; see also Ndoye et al. (2017); Chabert et al. (2023)); ii) a relatively warm inshore strip over the inner shelf where bottom friction checked Ekman dynamics (through merging of the surface and bottom boundary layers (Estrade et al., 2008)) and enhanced residence times; iii) a warm anticyclonic meander/eddy that frequently impinged onto the continental shelf south of Dakar and whose southern edge coincides with a recurrent upwelling filament responsible for offshore export. These patterns resulted to a large extent from the continental shelf widening near 14.5°N where preferential onshore water transport took place (Ndoye et al., 2017; Pringle, 2002). Our model was able to qualitatively reproduce these patterns and their disturbances by synoptic wind fluctuations with a degree of realism that we deemed sufficient to deserve analysis of its coupled biogeochemical solutions.

The zonation of the SSUS mean biogeochemical fields was also evident in Fig. 1. Elevated nitrate concentrations and low SST were essentially colocated near the 20 m isobath while the inner shelf was depleted of nitrate. The largest plankton concentrations were also located near the 20 m isobath, albeit a bit on its onshore side north of 13.5-14°N (see Figs. 1b-f, note that all planktonic variables were converted from carbon to nitrogen units using the model Redfield ratio 122/16 to facilitate comparison with nitrate). We interpreted this as a consequence of enhanced retention and regenerated primary production over the inner shelf.

The distribution of biogeochemical tracers revealed interesting alongshore structures consistent with upwelling of nutrient-rich waters being concentrated just south of the peninsula (Figs. 1d and 2d green line), and robust southward advection (Figs. 1a and 2a green line) while bottom-up trophic transfer occurred.

Along this advection route, the temporal lags associated with the propagation of synoptic nutrient anomalies through the trophic chain produced alongshore shifts in the plankton patterns. The fast-growing NANO peaked earlier in time than the other plankton species, thus upstream (north) along the mean advection pathway. Because of grazing, a relatively low NANO (resp. MICRO) abundance was also found in the latitude range 13.5-14.2°N (resp. 13-13.5°N) where MICRO and MESO (resp. MESO) concentrations became elevated. Overall, Figs. 1 and 2 revealed spatial oscillations in plankton abundance which seemed consistent with prey-predator dynamics (Edwards & Brindley, 1996). Additionally, we noted the unsurprising dominance of DIA over NANO in the nutrient-rich coastal area (Fig. 1b,e; Hutchings et al. (1995); Irigoien et al. (2005)) and the modest role seemingly played by the cold filament (situated near 13.5-14°N) on plankton export. We saw the latter as a direct consequence of having high plankton concentrations slightly inshore of the cold plume, i.e, more sheltered from the (sub)mesoscale export currents than the low temperature/high nutrient upwelled waters.

4 Responses to synoptic forcing perturbations

4.1 Domain-wide temporal response

Shelf-wide temporal responses of nitrate and plankton were examined by spatially averaging biogeochemical tracer concentrations over the entire shelf (between latitudes 13-14.75°N from the coast to the 100 m isobath; see grey box in Fig. 1a). The temporal modifications of concentration were robustly out of the range of their intrinsic variability (Figs. 2 and 3). Nitrate and plankton concentrations

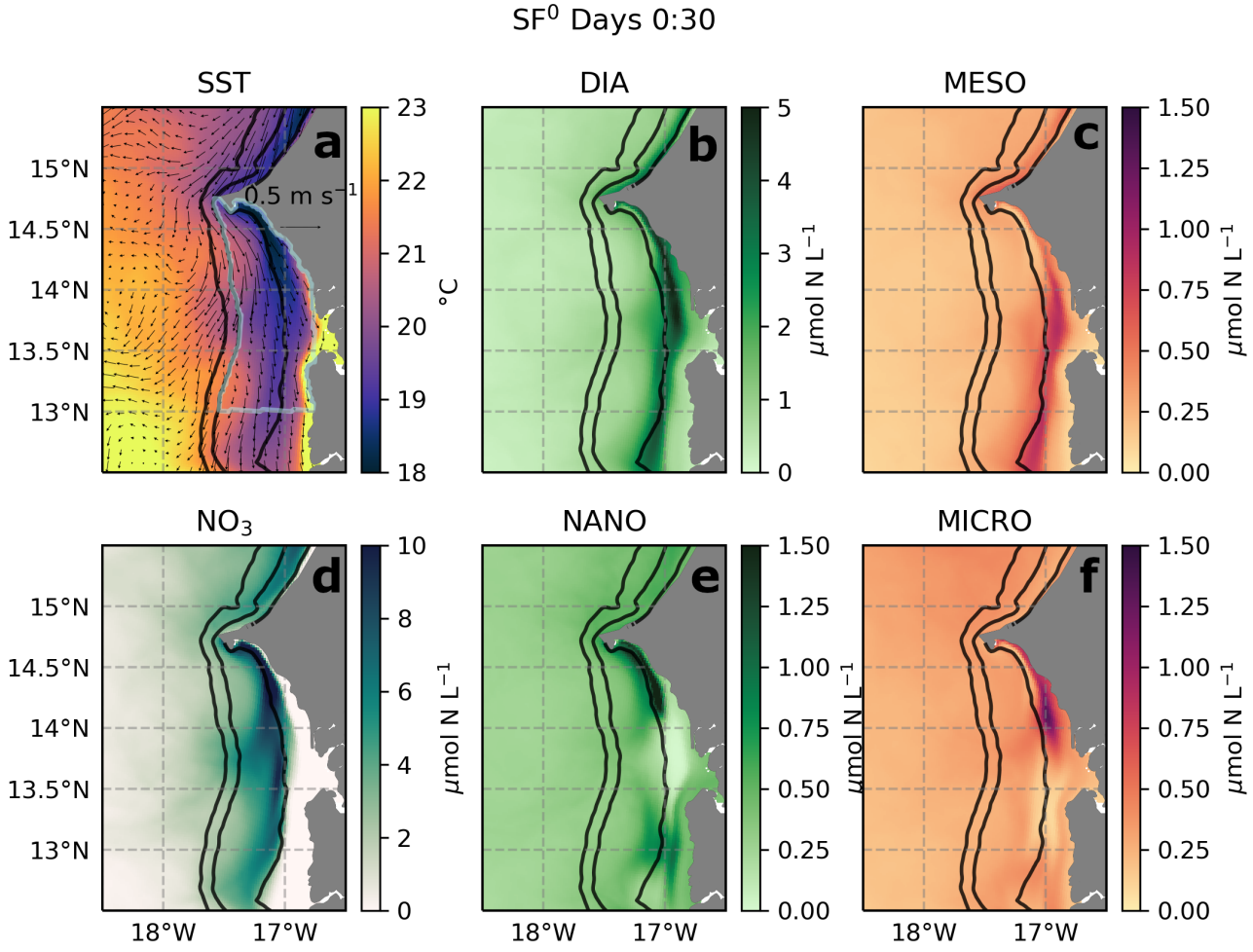

Figure 1: Surface patterns of SST (a), NO_3 (d), diatoms (b), nanophytoplankton (e), mesozooplankton (c) and microzooplankton (f) concentrations averaged over the ensemble for SF^0 between days 0 and 30. The box on which variables are averaged spatially is indicated with the light grey contour on panel a. The black lines indicate the 20, 100 and 500 m isobaths. Note that colorbar ranges are different for diatoms and nanophytoplankton. The Cape Verde (CV) is the land promontory extending westward at 14.7°N.

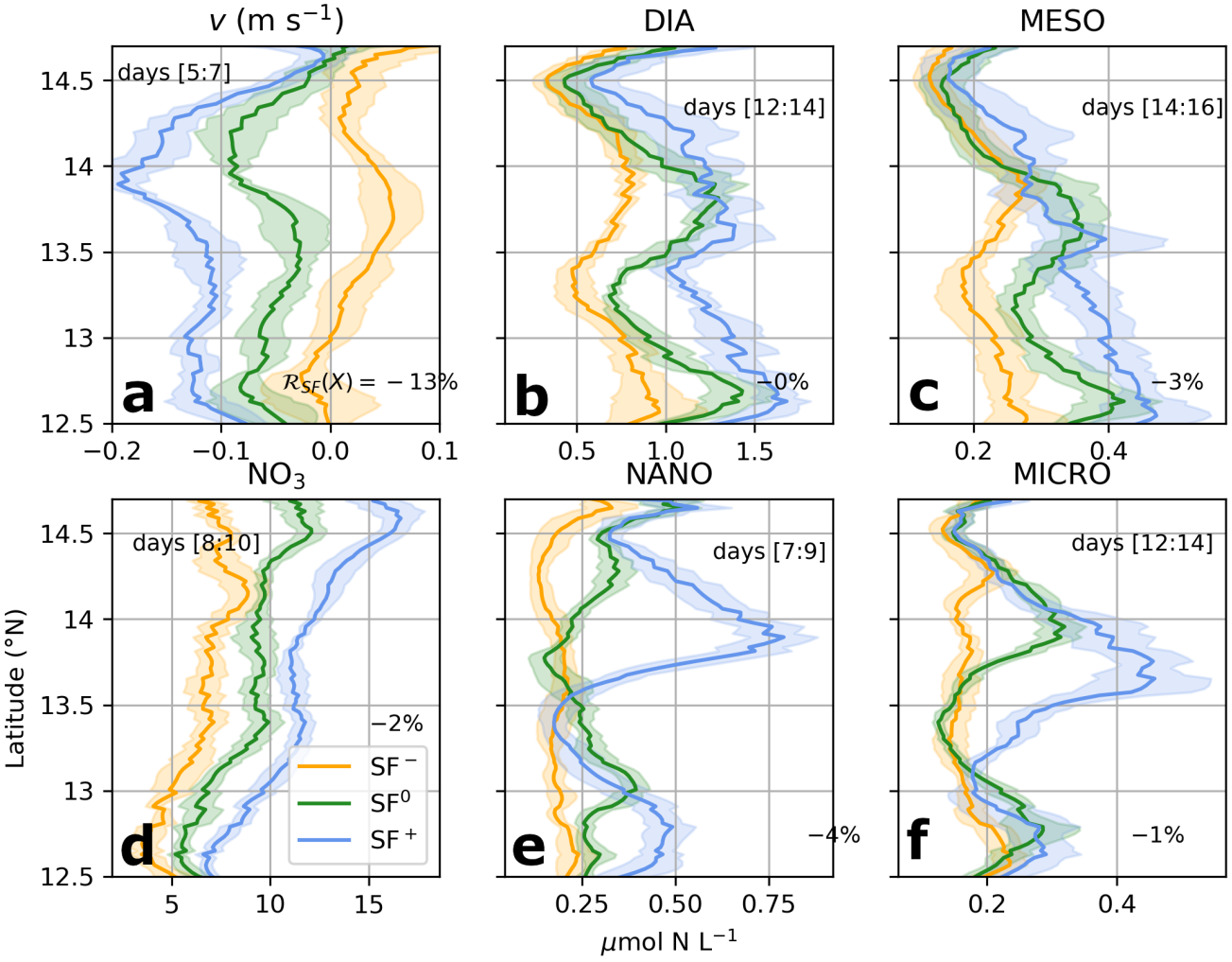

Figure 2: Meridional velocities (a), NO_3 (d), diatoms (b), nanophytoplankton (e), mesozooplankton (c) and microzooplankton (f) concentrations averaged over the entire shelf by latitude band (within the 100-0 m isobaths (see Fig.1) and from the bottom of the water column to the surface) and over the ensemble. SF^{-}, SF^{0} and SF^{+} are indicated in orange, green and blue lines; and the respective ensemble standard deviations are indicated by the shaded areas. $\mathcal{R}_{SF}$ (see section 2.5) is indicated for each quantity on the bottom right side of each panel. The temporal intervals $[t_1(X) : t_2(X)]$ used for averages are indicated in the upper part of each panels.

tended to increase during SF^+ and decrease during SF^-, but magnitudes, time scales/timing relative to that of the forcing anomaly, and details of synoptic responses were specific to each variable (see Fig. 3). In particular, plankton responses to $SF^\pm$ included several large oscillations unseen in the wind forcing anomalies and nutrient response.

We start with the timing sequence. For SF^+, the maximum value of nitrate was reached at day 9, nanophytoplankton at day 11, diatoms at day 13, microzooplankton at day 15 and mesozooplankton at day 17 (each planktonic extremum was reached broadly ~2 days earlier for SF^-). All plankton concentrations (except nanophytoplankton) presented first a weak decrease (resp. increase) in the first days of SF^+ (resp. SF^-), followed by a strong increase (resp. decrease) toward and after the end of the wind perturbation. The small early peaks appeared on time scales shorter than those of planktonic growth and were thus driven by ocean physics as an examination of budget terms revealed (Fig. 4; net tendencies in plankton concentration evolved mainly due to changes in the physics during the first days of the synoptic perturbation). The underlying process could only be the synoptic modulation of lateral tracer fluxes in and out of our continental shelf control volume because budgets in Fig. 4 were vertically averaged and therefore unaffected by vertical processes. NANO behaved differently because its shorter growth time scale left little time for advection processes to dominate. Conversely, longer growth time scales associated with large plankton (DIA and MESO) were consistent with their slower responses to the main nutrient perturbation, relative to those of small plankton groups NANO and MICRO (Fig. 3; and see section 5).

Another interesting aspect of the plankton response concerned the transition from SF^- back to climatological conditions for NANO and MICRO, which exhibited an additional oscillation in the form of an upward production rebound. This oscillation was absent in SF^+ whose intensification peak was, on the other hand, more pronounced than the main relaxation trough in SF^-, hence a substantial SF^+/SF^- asymmetry overall (see Fig. 3k,l).

Inspection of the budget terms indicated that a transient F^{Bio}_{NANO} excess around days 12-18 drove this SF^- extra oscillation (see Fig. 4d). Conversely, ocean physics could not be an important driver since F^{Phy}_{NANO} remained a one-signed (positive) anomalous source of NANO over the entire simulation. Given this and the appropriate phase relationship between NANO and its predators, we thus concluded that our synoptic forcing acted at temporal scales such that a (damped) prey-predator oscillation (Edwards & Brindley, 1996; Wang & Mu, 2014; Blasius et al., 2020) was produced between NANO and its fast predator MICRO. Constraints on ocean physics must however exist to allow a 0-D prey-predator interaction to

take place in a 3-D moving environment where advection and mixing can weaken the strength of trophic coupling. In fact, note that F_{NANO}^{Phy} did change sign and appeared in phase opposition relative to F_{NANO}^{Bio} during SF^+ simulations (see Fig. 4f). This is how we rationalize the fact that no post-intensification NANO-MICRO (negative) oscillation was found in SF^+ simulations, in which the circulation was significantly more energetic than in SF^- (Fig. 3a).

Stronger currents in SF^+ leading to weaker trophic coupling/top-down control could also explain the more intense forced reaction of NANO to SF^+ than SF^- (with respective $\mathcal{W}^+$ and $\mathcal{W}^-$ values of 46 and 35 %). On the other hand, PISCES has several nonlinear features that prevent phytoplankton concentrations from becoming too low (grazing refuge, density dependant mortality) and could be responsible for this asymmetry. Untangling these physical and biogeochemical reasons would require sensitivity runs.

We finish this section with a more quantitative assessment of asymmetries relative to the climatological reference state. In Fig. 3d-f,j-l we show the evolution of the cumulative asymmetry index $\mathcal{S}_{SF}$ (see section 2 on methods). We have previously established in Chabert et al. (2023) that meridional velocities exhibited the strongest asymmetries of all model physical variables, with $\mathcal{S}_{SF}(v)$ of the order of 10% (Fig. 3d). Biogeochemical asymmetries were systematically lower than the latter, in particular at final time. The ensemble spread was also quite diminished. And note that, despite being visually quite affected by perturbations of the flow field, nitrate presented strikingly low asymmetry at SSUS scale ($< 2\%$). Despite using intense wind perturbations (see section 2), the nonlinearities susceptible to produce $SF^{\pm}$ asymmetries, *e.g.*, through tracer advection, entrainment/detrainment in and out of the mixed layer, or biogeochemical reactions, were thus essentially muted from a SSUS-wide system perspective.

4.2 Alongshore structure of the response

$SF^{\pm}$ perturbations modified the spatial distribution of plankton concentrations and in particular their alongshore modulation described in section 3 (Fig. 2). $SF^{\pm}$ anomalies are shown for the 2-day period during which they were the most pronounced. All ecosystem quantities were significantly perturbed spatially at these times.

During SF^+, the most perturbed quantities were the concentrations of small plankton classes. The NANO concentration maximum shifted southwards from 14.25 to 13.8°N (~50 km) and tripled in amplitude. The peak in MICRO shifted from 14 to 13.6°N and increased by ~50% compared to SF^0. It

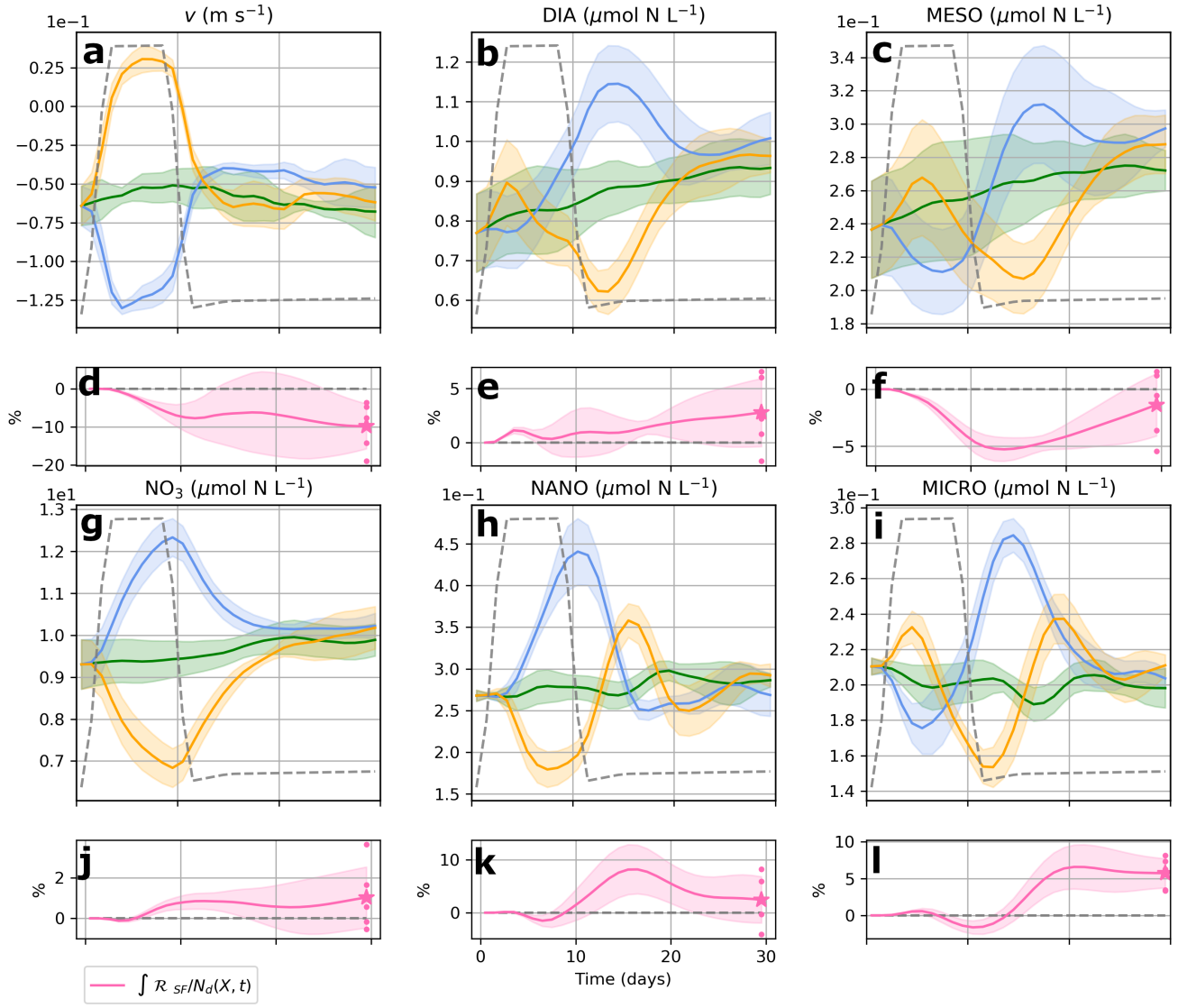

Figure 3: Meridional velocities (a), NO_3 (g), diatoms (b), nanophytoplankton (h), mesozooplankton (c) and microzooplankton (i) concentrations averaged over the entire shelf, water column, and over the ensemble. Green, orange and blue lines indicate SF^0, SF^- and SF^+. Shaded areas indicate the ensemble standard deviation. The box of integration is shown on Fig. 1a (grey contour between 13-14.75°N and 0-100 m isobaths). Time series of $\int \mathcal{R}_{SF}/N_d$ (with N_d the number of days) diagnose the perturbations asymmetries and are shown for each variable X in pink in panels (d-f,j-l); the value of each member of the ensemble at day 30 is indicated by a pink dot; each residual diagnostic panel is located below the panel showing the evolution of variable X. The grey dashed line indicates the amplitude modulation of the wind fluctuations. Note the different y-axis scales indicated on the top left of each panel.

even slightly exceeded the mesozooplankton concentration at this location. In contrast, changes in the concentration of DIA and MESO occurred mostly south of 13.5°N. All this was consistent with the notable increase in southward current (Fig. 2a) and its Lagrangian implications for the spatial organization of trophic transfers. In the same spirit, note the small spatial shift between the SF^+ peaks in NANO (13.9°N) and MICRO (13.6°N), its main grazer.

During SF^-, all spatial oscillations were damped such that plankton concentrations were more homogeneous over the shelf compared to SF^0. Currents were weaker and also more variable in SF^-, particularly in the south (Chabert et al., 2023). Modest peaks in DIA and MESO remained noticeable but their location was shifted northward compared to SF^0, again in agreement with the meridional (northward) flow anomaly.

5 Propagation of physical perturbations through the planktonic ecosystem

In this section, we investigate the trophic propagation of the disturbances to assess whether the bottom-up perturbations are amplified or damped from one system level to the next. Fig. 5 displays $\mathcal{W}^{\pm}$, the relative amplitude of the synoptic perturbations over the most perturbed period of the simulation (see section 2) for the key variables concerned. The maximum amplitude of the absolute perturbations and the underlying perturbations of transfer rates are also informative of trophic propagation (see Figs. 3 and 4). We start with the transfer of the perturbation from wind to NO_3 enrichment. Based on a conceptual Ekman/Bakun type model a classical *a priori* assumption to be used as a strawman is that $\mathcal{W}^{\pm}$ for wind stress and physical nitrate flux into the control volume ($F^{Phy}_{NO_3}$) are linearly related (Messié et al., 2009); see for instance (Jacox et al., 2018; Jorgensen et al., 2024) for a more elaborate approach). Reasoning on SF^+, this would imply that increasing wind intensity by 60% leads to a relative increase of $F^{Phy}_{NO_3}$ by a similar figure, and likewise in terms of decrease for SF^-. In contrast, the system response was characterized by the fact that: i) $\mathcal{W}^{\pm}(F^{Phy}_{NO_3})$ reached $\sim \pm$ 100% at day 3 (compare panels a and c in Fig. 4 to panel b), *i.e.*, wind perturbations were initially more effective in terms of NO_3 enrichment than the climatological wind; ii) the extra NO_3 enrichment associated with the wind perturbation rapidly diminished. Alongshore adjustment of the pressure field (sea level) by coastal trapped waves is an important factor shaping the response of coastal systems to wind forcing at various time scales (Philander & Yoon, 1982; Ndoye et al., 2017; Colas et al., 2008). The early response of $F^{Phy}_{NO_3}$ to SF+/SF-

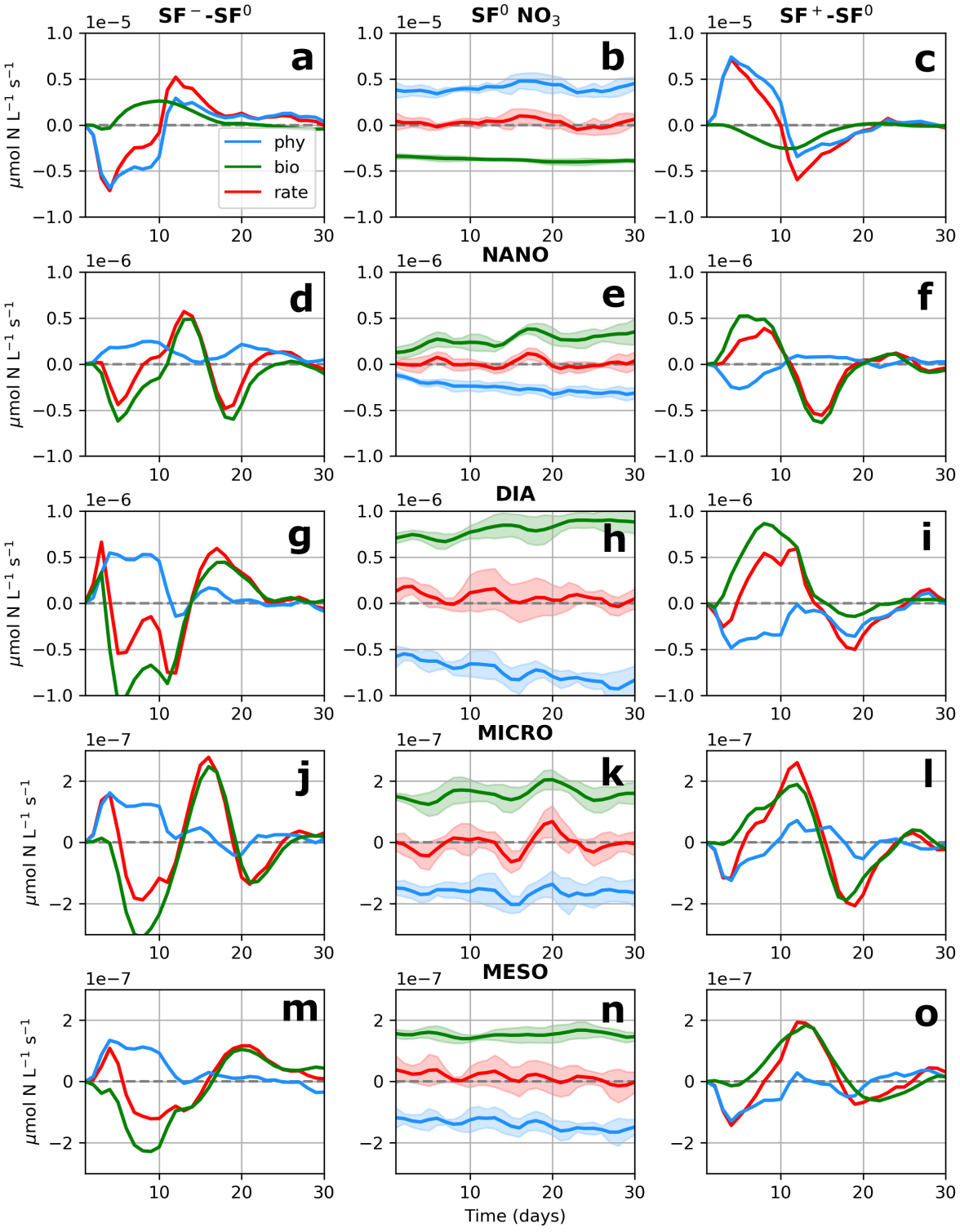

Figure 4: Time series of tendency terms of the biogeochemical tracer budgets (red line) along with their decomposition into a physical (blue lines) and biogeochemical (green lines) contribution. Spatial averaging is performed over the continental shelf (h<100m) south of the Cape Verde peninsula (see green box in Fig.1a). The three columns represent the anomaly SF^{-}-SF^{0} (left), the climatological simulations SF^{0} (middle) and the anomaly SF^{+}-SF^{0} (right). The rows correspond (from top to bottom) to NO_3, NANO, DIA, MICRO and MESO.

was presumably influenced by this process.

Moving up in the trophic chain, we turn to the implications of this change in nutrient stock and enrichment rate for the plankton ecosystem. We start by noting that the magnitude of the perturbations for the biological quantities was a moderate fraction of those for NO_3. For example, the net NO_3 uptake perturbation by the plankton ecosystem $\int F_{NO_3}^{Bio}(t)\,dt$ was ~50% of the total physical enrichment perturbation between days 0 and 10 (the remainder ~50% was disposed of after day 10 by the physics - see Fig. 4a,c). Likewise, biomass perturbations (in nitrogen units) were only a small fraction of the ones for the nutrient stock (7-9% for phytoplankton; 2-3% for zooplankton).

Overall, the examination of $\mathcal{W}^{\pm}$ for plankton abundance (Fig. 5) revealed a moderate attenuation of the perturbation amplitudes from phytoplankton to zooplankton (*e.g.*, from $\mathcal{W}^{\pm}$(DIA)≈30% to $\mathcal{W}^{\pm}$(MESO)≈20%), with an exception for small planktons NANO and MICRO in SF^{+} (see above section 4.2 for our explanation invoking scrambling of trophic links by SF^{+} intense ocean physics). A large dispersion of the small plankton responses can be observed among the ensemble, contrasting with the larger plankton boxes.

The attenuation of the perturbation as it propagated up the foodchain contrasted with the trophic amplifications found in some previous studies (Chenillat et al., 2013; Kwiatkowski et al., 2019). This was despite our biogeochemical model having a non predatory linear loss term for zooplankton, which is known to favor trophic amplification, at least in equilibrium conditions (Kwiatkowski et al., 2019). Here though, the duration of the nutrient input pulse/deficit (~10 days) was too short to let MESO reach equilibration with the (transient) $SF^{\pm}$ conditions (for example, note how NO_3 concentrations had already nearly returned to climatology at day 15 when MESO was peaking; see Figs. 3c,g).

In summary, it thus appears that our relatively long synoptic events (by West African standards) were not particularly apt at stimulating large plankton responses, particularly along the so-called short food chain (nutrients to diatoms to copepods; (Kämpf & Chapman, 2016)).

6 Discussion and conclusions

Modest impact of synoptic variability on the SSUS ecosystem

Overall, our findings support the general idea that synoptic fluctuations produce modest disturbances in a coastal upwelling sector like the SSUS. The propagation of our idealized synoptic perturbations in the plankton model was characterized by: a large degree of relaxation-intensification symmetry (hence

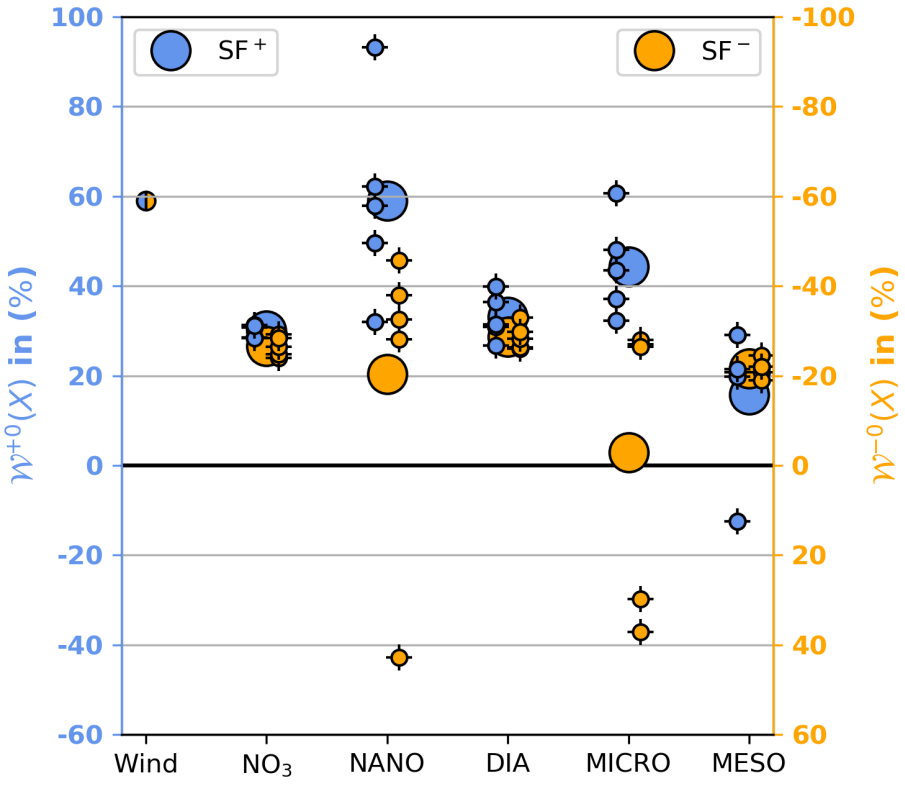

Figure 5: Magnitude $\mathcal{W}^{\pm 0}(X)$ of SF^{+} (blue, left axis) and SF^{-} (orange, right axis) perturbations along biogeochemical and biological levels over the shelf south of Cape Verde peninsula (h< $100m$, see Fig. 1a) . Smaller dots indicate ensemble members, larger dots indicate ensemble averages. Note the large dispersion for the small plankton (NANO and MICRO) responses.

limited potential for net rectification associated with variability in this scale range); a mild trophic attenuation; a low transfer efficiency of the synoptic nitrate perturbation into plankton biomass. All these characteristics were a priori specific to the SSUS geomorphology and dynamical regime (and also presumably dependent on our choice of model parameters).

Some of our findings may seem in apparent contradiction with existing evidence that synoptic variability/intermittency plays an important role in the functioning of upwelling ecosystems, most notably in sectors like ours where headlands and bays promote the existence of robust/frequent retentive circulation features (Vander Woude et al., 2006). Specifically, the role of relaxation episodes found to be essential in some sectors (Dugdale et al., 2006; Burger et al., 2020; Wilkerson et al., 2006) (Burger et al., 2020) was not evidenced herein. Several comments are in order to help clarify this.

First, many of the studies supporting the view that synoptic variability is important are concerned with the reproduction success of species with egg/larval planktonic stages and specific recruitment requirements (Pfaff et al., 2015; Menge & Menge, 2013) such as the necessity to settle nearshore. Typically, the success metrics demands that the scale of the organism's drift $L_{drift} = \int_{t0}^{t0+T_{eco}} u(x(t), y(t), z(t))dt$ be commensurate with the cross-shore width of the coastal habitat suitable for the organism under consideration, where T_{eco} is the duration of the ecological process under consideration (*e.g.*, larval/planktonic life stage), u is the cross-shore horizontal current field, initial release points $[x(t_0),y(t_0)]$ cover the coastal spawning areas, and z(t) is determined by organism behavior. The integral is computed along the Lagrangian trajectory followed by organisms. This framework is also appropriate when considering the primary production available to the ecosystem of continental shelves (Botsford et al., 2006). In sectors with strong climatological winds and/or a narrow continental shelf, recruitment success can only be achieved intermittently when cross-shore transport compensations occur thanks to variability of the velocity field in time, and/or in space (e.g, mesoscale turbulence). Synoptic variability then produces temporal windows that, despite their shortness, are essential because they make recruitment success non-zero. Note that wind synoptic variability can also help to meet recruitment success requirements which call for limited alongshore displacements from spawning to recruitment, when alongshore habitat heterogeneities exist due to the nature of the bottom substrate or prevailing thermohaline conditions. In contrast to large parts of the Californian, Chilean, and South African upwelling systems, the SSUS is characterized by a wide continental shelf and regional alongshore pressure gradients that favor smaller L_{drift} values/longer coastal retention. This is, we think, the main reason why the SSUS was only modestly sensitive to wind synoptic variability.

	P^+ / P^-	P^+ / P^-	P^+ / P^-
T_{avg} (days)	5	10	20
Occurrence	**15 % / 9%**	**6% / 2.5%**	6% / 2.5%
Perturbation (N m^{-2})	±0.032	±0.032	±**0.025**

Table 1: Probability of exceeding a wind intensification/relaxation perturbation (P^+/P^-) threshold over a T_{avg}-long period during the upwelling season (December-May years 2000-2010). Wind perturbation statistics are computed by time-averaging a low-pass filtered time series of ERA5 wind stress in the box (-19°E, -16.5°E, 12.5°N, 15.5°N) over all possible T_{avg}-long time windows that start at 12PM (i.e., two consecutive windows overlap over T_{avg}-1 days). We use a Butterworth filter with a threshold period of 115 days for low-pass filtering. For each column, the row with the values in bold is the one deduced after having fixed the other two rows. Thus, for example, 20 day-long wind perturbations with a probability of occurrence similar to the one of the 10-day long $SF^{\pm}$ used in this study would have a magnitude of ±0.025 N m^{-2}, i.e. 25% less than $SF^{\pm}$. Similar results were obtained with a threshold period of 60 days for low-pass filtering.

Second, although our choices for intensity and duration of the wind stress perturbations made our study cases quite extreme (see section 2 and Table 1), we only considered one simple form of synoptic disturbance. Compound events such as intensification-relaxation sequences would be interesting to study. Longer events (*e.g.* ∼20 days) would have a greater impact on plankton dynamics but, in a system like the SSUS, the typical magnitude of the wind perturbation would be smaller (see Table 1). Running simulations with a complex/realistic wind history will be useful to identify synoptic outlier events (Jönsson & Salisbury, 2016). On the basis of (Thomsen et al., 2021), we presume that air-sea heat exchanges cooling the ocean (more than in the present SF experiments) could substantially affect the synoptic response of plankton.

Third, note that we have presented a shelf-wide view of synoptic effects while the response of the inner shelf appeared stronger and more nonlinear in nutrients, NANO and MICRO (*e.g.* the SF^+ perturbation peak for NO_3 was nearly three times larger than over the entire shelf and thus larger than the atmospheric perturbation amplitude, not shown). $SF^{\pm}$ asymmetries were also amplified over the inner shelf considered in isolation, particularly for small plankton classes. The inner shelf planktonic ecosystem may have been oversimplified in our simulations due to the absence of explicit cyanobacteria in our model providing diatoms with ammonium in the surface layer (Bonnet et al., 2016) or sedimentary

sources of nutrients.

Finally, a representation of zooplankton involving several life stages (including dormance/diapause) and diel vertical migration behavior would enhance the richness of and nonlinearities in physics-plankton interactions and trophic coupling. Having some ontogenetic time scales in the synoptic range would presumably magnify the effect of the latter in our system.

Realism of the model synoptic behavior: Plankton concentration oscillations

Whether biogeochemical models have appropriate functional forms to represent biological reactions, and what implications model choices have on model behavior, are long-standing issues in biogeochemical modeling (Hallam, 1978; Steele & Henderson, 1992; Franks, 2009), particularly with regard to the tendency of models to produce (or not) predator-prey oscillations (Gentleman & Neuheimer, 2008). Our simulations showed weak oscillations despite substantial perturbations in nitrate flux (Fig. 4). In its design PISCES incorporates two standard stabilizing features: a 4 plankton group ecosystem connected via multiple feeding pathways and a quadratic predation-type closure for zooplankton. It nevertheless produced some manifestation of mild prey-predator interactions as a response to synoptic forcing fluctuations and also in steady state following advection pathways emanating from the upwelling source. Multi-year simulations with realistic forcings could reveal if the latter have a chance to be observed in the real ocean. If so, two moorings with physics and biogeochemical sensors located over the transition inner-to-mid shelf at two latitudes judiciously chosen could provide an interesting model evaluation and, perhaps a way to make progress.

Furthermore, testable patterns of model synoptic responses could be uncovered for other upwelling sectors, in particular where synoptic activity is consistently paced by intra-seasonal atmospheric modes (as is the case in the southern hemisphere mid-latitude sectors, *e.g.* (Dewitte et al., 2011) in the Peru upwelling system).

Realism of the model synoptic behavior: Nanophytoplankton vs diatoms

The fact that the planktonic response to synoptic events involved nanoplankton and diatoms in roughly equal proportions (for example, both compartments captured similar amounts of the excess nutrients associated with SF^{+}) may seem at odds with what is known about plankton in upwelling systems and more generally (Sommer et al., 2002; Ferreira et al., 2020; Ward et al., 2014). Model parameters could be tuned differently so as to favor the diatom's response. Most simply, the NANO growth (resp., microzoplankton predation on NANO) rate could be diminished (resp. increased). However, this would

also decrease the mean NANO biomass which was a factor ~ 3 smaller than DIA biomass in our simulations (Fig. 3), at odds with preliminary observation-based estimates (E. Machu, unpublished data) Alternatively, we recognize that some of the physiological features susceptible to provide diatoms with a competitive advantage were not included in PISCES: a faster response time to changing environmental conditions (e.g, surge uptake and/or large nutrient stores (Fawcett & Ward, 2011; Lampe et al., 2021)); an ability to sustain high growth rates on NO_3, *e.g.*, due to lower metabolic cost or greater uptake capacity (Marañón, 2015).

A plea for coordinated modeling experiments across upwelling systems

(Chabert et al., 2023) and the present study offer a reproducible framework that can be implemented in or adapted to other upwelling sectors and other modelling systems (*e.g.*, to explore sensitivity to biogeochemical model parameterizations). We believe that this would provide new insight and research avenues pertaining to the functioning of upwelling ecosystems. Such a synoptic "initiative" may not provide direct answers to our most pressing science questions, which mainly concern longer time scales. But as a trial run, it would generally contribute to advancing coastal plankton ecosystem models. Such an initiative would also be timely, with the mounting impacts of (and interest in) extreme marine events, many of which are in the synoptic scale range (Pietri et al., 2021), or intermittently aggravated/mitigated and possibly initiated by synoptic events (Dalsin et al., 2023). Dissolved oxygen dynamics are also strongly modulated on synoptic time scales (Machu et al., 2019; Tall et al., 2021; Adams et al., 2013; Galán et al., 2020; Frieder et al., 2012), with potentially widespread consequences on higher trophic levels. We provide a toolkit to facilitate the implementation of synoptic sensitivity frameworks similar to ours in other systems (`https://github.com/pierrechabert/toolkit_windevents`). Ultimately, our hope is that this will spawn a line of coordinated comparison studies across systems, exploring synoptic scales and beyond.

Funding

PC was funded by a PhD grant from IPSL EUR. This work was supported by IRD laboratoire mixte international ECLAIRS2 and LEFE PISCO. Model simulations were performed on the Irene skylake TGCC HPC under DARI projects A0110101140 and A0130101140.

Data Archiving

Given the large size of the dataset (~ 2 TB), it is not stored online. The data can be made available upon request to the authors.

References

Adams, K. A., Barth, J. A., & Chan, F. (2013). Temporal variability of near-bottom dissolved oxygen during upwelling off central oregon. *Journal of Geophysical Research: Oceans*, *118*(10), 4839–4854.

Aguirre, C., Garreaud, R., Belmar, L., Farías, L., Ramajo, L., & Barrera, F. (2021). High-Frequency Variability of the Surface Ocean Properties Off Central Chile During the Upwelling Season. *Frontiers in Marine Science*, *8*. Retrieved 2022-09-02, from https://www.frontiersin.org/articles/10.3389/fmars.2021.702051

Aumont, O., Ethé, C., Tagliabue, A., Bopp, L., & Gehlen, M. (2015, August). PISCES-v2: an ocean biogeochemical model for carbon and ecosystem studies. *Geoscientific Model Development*, *8*(8), 2465–2513. Retrieved 2022-09-29, from https://gmd.copernicus.org/articles/8/2465/2015/ (Publisher: Copernicus GmbH) doi: 10.5194/gmd-8-2465-2015

Barnier, B., Siefridt, L., & Marchesiello, P. (1995, June). Thermal forcing for a global ocean circulation model using a three-year climatology of ECMWF analyses. *Journal of Marine Systems*, *6*(4), 363–380. Retrieved 2021-11-22, from https://www.sciencedirect.com/science/article/pii/0924796394000349 doi: 10.1016/0924-7963(94)00034-9

Blasius, B., Rudolf, L., Weithoff, G., Gaedke, U., & Fussmann, G. F. (2020). Long-term cyclic persistence in an experimental predator–prey system. *Nature*, *577*(7789), 226–230.

Bonnet, S., Berthelot, H., Turk-Kubo, K., Cornet-Barthaux, V., Fawcett, S., Berman-Frank, I., ... Capone, D. G. (2016). Diazotroph derived nitrogen supports diatom growth in the south west pacific: A quantitative study using nanosims. *Limnology and Oceanography*, *61*(5), 1549-1562. Retrieved from https://aslopubs.onlinelibrary.wiley.com/doi/abs/10.1002/lno.10300 doi: https://doi.org/10.1002/lno.10300

Botsford, L. W., Lawrence, C. A., Dever, E. P., Hastings, A., & Largier, J. (2003). Wind strength and biological productivity in upwelling systems: an idealized study. *Fisheries Oceanography*, *12*(4-5), 245–259. Retrieved 2022-07-22, from https://onlinelibrary.wiley.com/doi/abs/10.1046/j.1365-2419.2003.00265.x (_eprint: https://onlinelibrary.wiley.com/doi/pdf/10.1046/j.1365-2419.2003.00265.x) doi: 10.1046/j.1365-2419.2003.00265.x

Botsford, L. W., Lawrence, C. A., Dever, E. P., Hastings, A., & Largier, J. (2006, December). Effects of variable winds on biological productivity on continental shelves in coastal upwelling systems. *Deep Sea Research Part II: Topical Studies in Oceanography*, *53*(25-26), 3116–3140. Retrieved 2022-09-29, from https://linkinghub.elsevier.com/retrieve/pii/S0967064506002281 doi: 10.1016/j.dsr2.2006.07.011

Burger, J. M., Moloney, C. L., Walker, D. R., Parrott, R. G., & Fawcett, S. E. (2020). Drivers of short-term variability in phytoplankton production in an embayment of the southern benguela upwelling system. *Journal of Marine Systems*, *208*, 103341.

Capet, X., Estrade, P., Machu, E., Ndoye, S., Grelet, J., Lazar, A., ... Brehmer, P. (2017, January). On the Dynamics of the Southern Senegal Upwelling Center: Observed Variability from Synoptic to Superinertial Scales. *Journal of Physical Oceanography*, *47*(1), 155–180. Retrieved 2021-11-22, from https://journals.ametsoc.org/view/journals/phoc/47/1/jpo-d-15-0247.1.xml (Publisher: American Meteorological Society Section: Journal of Physical Oceanography) doi: 10.1175/JPO-D-15-0247.1

Carton, J. A., & Giese, B. S. (2008, August). A Reanalysis of Ocean Climate Using Simple Ocean Data Assimilation (SODA). *Monthly Weather Review*, *136*(8), 2999–3017. Retrieved 2021-11-22, from https://journals.ametsoc.org/view/journals/mwre/136/8/2007mwr1978.1.xml (Publisher: American Meteorological Society Section: Monthly Weather Review) doi: 10.1175/2007MWR1978.1

Chabert, P., Capet, X., Echevin, V., Lazar, A., Hourdin, C., & Ndoye, S. (2023, March). Impact of Synoptic Wind Intensification and Relaxation on the Dynamics and Heat Budget of the South Senegalese Upwelling Sector. *Journal of Physical Oceanography*, *53*(4), 1041–1067. Retrieved 2023-03-22, from

https://journals.ametsoc.org/view/journals/phoc/53/4/JPO-D-22-0092.1.xml (Publisher: American Meteorological Society Section: Journal of Physical Oceanography) doi: 10.1175/JPO-D-22-0092.1

Chabert, P., d'Ovidio, F., Echevin, V., Stukel, M. R., & Ohman, M. D. (2021). Cross-Shore Flow and Implications for Carbon Export in the California Current Ecosystem: A Lagrangian Analysis. *Journal of Geophysical Research: Oceans*, *126*(2), e2020JC016611. Retrieved 2022-07-22, from https://onlinelibrary.wiley.com/doi/abs/10.1029/2020JC016611 (_eprint: https://onlinelibrary.wiley.com/doi/pdf/10.1029/2020JC016611) doi: 10.1029/2020JC016611

Chavez, F. P., & Messié, M. (2009, December). A comparison of Eastern Boundary Upwelling Ecosystems. *Progress in Oceanography*, *83*(1), 80–96. Retrieved 2022-10-12, from https://www.sciencedirect.com/science/article/pii/S0079661109000998 doi: 10.1016/j.pocean.2009.07.032

Chenillat, F., Rivière, P., Capet, X., Franks, P. J. S., & Blanke, B. (2013, May). California Coastal Upwelling Onset Variability: Cross-Shore and Bottom-Up Propagation in the Planktonic Ecosystem. *PLOS ONE*, *8*(5), e62281. Retrieved 2022-07-22, from https://journals.plos.org/plosone/article?id=10.1371/journal.pone.0062281 (Publisher: Public Library of Science) doi: 10.1371/journal.pone.0062281

Colas, F., Capet, X., Mcwilliams, J. C., & Shchepetkin, A. (2008). 1997–1998 el niño off peru: A numerical study. *Progress in Oceanography*, *79*(2-4), 138–155.

Dalsin, M., Walter, R. K., & Mazzini, P. L. (2023). Effects of basin-scale climate modes and upwelling on nearshore marine heatwaves and cold spells in the california current. *Scientific reports*, *13*(1), 12389.

Debreu, L., & Blayo, E. (2008, December). Two-way embedding algorithms: a review. *Ocean Dynamics*, *58*(5), 415–428. Retrieved 2022-01-11, from https://doi.org/10.1007/s10236-008-0150-9 doi: 10.1007/s10236-008-0150-9

Desbiolles, F., Blanke, B., & Bentamy, A. (2014). Short-term upwelling events at the western African coast related to synoptic atmospheric structures as derived from satellite observations. *Journal of Geophysical Research: Oceans*, *119*(1), 461–483. Retrieved 2021-11-22, from https://onlinelibrary.wiley.com/doi/abs/10.1002/2013JC009278 (_eprint: https://onlinelibrary.wiley.com/doi/pdf/10.1002/2013JC009278) doi: 10.1002/2013JC009278

Dewitte, B., Illig, S., Renault, L., Goubanova, K., Takahashi, K., Gushchina, D., . . . Purca, S. (2011).

Modes of covariability between sea surface temperature and wind stress intraseasonal anomalies along the coast of peru from satellite observations (2000–2008). *Journal of Geophysical Research: Oceans*, *116*(C4). Retrieved from https://agupubs.onlinelibrary.wiley.com/doi/abs/10.1029/2010JC006495 doi: https://doi.org/10.1029/2010JC006495

Dugdale, R., Wilkerson, F., Hogue, V., & Marchi, A. (2006). Nutrient controls on new production in the bodega bay, california, coastal upwelling plume. *Deep Sea Research Part II: Topical Studies in Oceanography*, *53*(25-26), 3049–3062.

Echevin, V., Hauschildt, J., Colas, F., Thomsen, S., & Aumont, O. (2021). Impact of Chlorophyll Shading on the Peruvian Upwelling System. *Geophysical Research Letters*, *48*(19), e2021GL094429. Retrieved 2022-09-17, from https://onlinelibrary.wiley.com/doi/abs/10.1029/2021GL094429 (_eprint: https://onlinelibrary.wiley.com/doi/pdf/10.1029/2021GL094429) doi: 10.1029/2021GL094429

Edwards, A. M., & Brindley, J. (1996, January). Oscillatory behaviour in a three-component plankton population model. *Dynamics and Stability of Systems*, *11*(4), 347–370. Retrieved 2023-05-17, from https://doi.org/10.1080/02681119608806231 (Publisher: Taylor & Francis _eprint: https://doi.org/10.1080/02681119608806231) doi: 10.1080/02681119608806231

Estrade, P., Marchesiello, P., De Verdière, A. C., & Roy, C. (2008, September). Cross-shelf structure of coastal upwelling: A two — dimensional extension of Ekman's theory and a mechanism for inner shelf upwelling shut down. *Journal of Marine Research*, *66*(5), 589–616. doi: 10.1357/002224008787536790

Evans, W., Hales, B., Strutton, P. G., Shearman, R. K., & Barth, J. A. (2015). Failure to bloom: Intense upwelling results in negligible phytoplankton response and prolonged CO2 outgassing over the Oregon shelf. *Journal of Geophysical Research: Oceans*, *120*(3), 1446–1461. Retrieved 2022-09-28, from https://onlinelibrary.wiley.com/doi/abs/10.1002/2014JC010580 (_eprint: https://onlinelibrary.wiley.com/doi/pdf/10.1002/2014JC010580) doi: 10.1002/2014JC010580

Fawcett, S., & Ward, B. (2011). Phytoplankton succession and nitrogen utilization during the development of an upwelling bloom. *Marine Ecology Progress Series*, *428*, 13–31.

Ferreira, A., Sá, C., Silva, N., Beltrán, C., Dias, A., & Brito, A. (2020). Phytoplankton response to nutrient pulses in an upwelling system assessed through a microcosm experiment (algarrobo bay,

chile). *Ocean & Coastal Management*, *190*, 105167.

Franks, P. J. S. (2009, November). Planktonic ecosystem models: perplexing parameterizations and a failure to fail. *Journal of Plankton Research*, *31*(11), 1299–1306. Retrieved 2022-10-12, from https://doi.org/10.1093/plankt/fbp069 doi: 10.1093/plankt/fbp069

Frieder, C., Nam, S., Martz, T., & Levin, L. (2012). High temporal and spatial variability of dissolved oxygen and ph in a nearshore california kelp forest. *Biogeosciences*, *9*(10), 3917–3930.

Fréon, P., Barange, M., & Arístegui, J. (2009, December). Eastern Boundary Upwelling Ecosystems: Integrative and comparative approaches. *Progress in Oceanography*, *83*(1), 1–14. Retrieved 2022-10-03, from https://www.sciencedirect.com/science/article/pii/S0079661109001323 doi: 10.1016/j.pocean.2009.08.001

Galán, A., Zirbel, M. J., Saldías, G. S., Chan, F., & Letelier, R. (2020). The role of upwelling intermittence in the development of hypoxia and nitrogen loss over the oregon shelf. *Journal of Marine Systems*, *207*, 103342.

Galán, A., Zirbel, M. J., Saldías, G. S., Chan, F., & Letelier, R. (2020, July). The role of upwelling intermittence in the development of hypoxia and nitrogen loss over the Oregon shelf. *Journal of Marine Systems*, *207*, 103342. Retrieved 2023-03-09, from https://www.sciencedirect.com/science/article/pii/S0924796320300385 doi: 10.1016/j.jmarsys.2020.103342

Garcia, H. E., Weathers, K., Paver, C. R., Smolyar, I., Boyer, T. P., Locarnini, R. A., . . . Reagan, J. (2018). *World Ocean Atlas 2018. Volume 4: Dissolved Inorganic Nutrients (phosphate, nitrate and nitrate+nitrite, silicate).* Retrieved 2021-06-05, from https://www.ncei.noaa.gov/archive/accession/NCEI-WOA18. (Publication Title: NOAA National Centers for Environmental Information. A. Mishonov Technical Ed.; NOAA Atlas NESDIS 84)

Gentleman, W., & Neuheimer, A. (2008). Functional responses and ecosystem dynamics: how clearance rates explain the influence of satiation, food-limitation and acclimation. *Journal of Plankton Research*, *30*(11), 1215–1231.

Gruber, N., Lachkar, Z., Frenzel, H., Marchesiello, P., Münnich, M., McWilliams, J. C., . . . Plattner, G.-K. (2011, November). Eddy-induced reduction of biological production in eastern boundary upwelling systems. *Nature Geoscience*, *4*(11), 787–792. Retrieved 2022-11-28, from

http://www.nature.com/articles/ngeo1273 doi: 10.1038/ngeo1273

Hallam, T. G. (1978). Structural sensitivity of grazing formulations in nutrient controlled plankton models. *Journal of Mathematical Biology*, *5*(3), 269–280.

Hauschildt, J., Thomsen, S., Echevin, V., Oschlies, A., José, Y. S., Krahmann, G., ... Lavik, G. (2021, June). The fate of upwelled nitrate off Peru shaped by submesoscale filaments and fronts. *Biogeosciences*, *18*(12), 3605–3629. Retrieved 2022-07-22, from https://bg.copernicus.org/articles/18/3605/2021/ (Publisher: Copernicus GmbH) doi: 10.5194/bg-18-3605-2021

Hersbach, H., Bell, B., Berrisford, P., Biavati, G., Horányi, A., Muñoz Sabater, J., ... Thépaut, J.-N. (2018). ERA5 hourly data on single levels from 1979 to present. Copernicus Climate Change Service (C3S) Climate Data Store (CDS). Retrieved 2020-12-15, from 10.24381/cds.adbb2d47

Hilt, M., Auclair, F., Benshila, R., Bordois, L., Capet, X., Debreu, L., ... Roblou, L. (2020, July). Numerical modelling of hydraulic control, solitary waves and primary instabilities in the Strait of Gibraltar. *Ocean Modelling*, *151*, 101642. Retrieved 2022-01-24, from https://www.sciencedirect.com/science/article/pii/S146350032030144X doi: 10.1016/j.ocemod.2020.101642

Hutchings, L., Pitcher, G., Probyn, T., & Bailey, G. (1995, January). The chemical and biological consequences of coastal upwelling. In (pp. 65–81).

Iles, A. C., Gouhier, T. C., Menge, B. A., Stewart, J. S., Haupt, A. J., & Lynch, M. C. (2012). Climate-driven trends and ecological implications of event-scale upwelling in the c alifornia c urrent s ystem. *Global Change Biology*, *18*(2), 783–796.

Irigoien, X., Flynn, K. J., & Harris, R. P. (2005, April). Phytoplankton blooms: a 'loophole' in microzooplankton grazing impact? *Journal of Plankton Research*, *27*(4), 313–321. Retrieved 2022-10-11, from https://doi.org/10.1093/plankt/fbi011 doi: 10.1093/plankt/fbi011

Jacox, M. G., & Edwards, C. A. (2011). Effects of stratification and shelf slope on nutrient supply in coastal upwelling regions. *Journal of Geophysical Research: Oceans*, *116*(C3). Retrieved 2022-03-22, from https://onlinelibrary.wiley.com/doi/abs/10.1029/2010JC006547 (_eprint: https://onlinelibrary.wiley.com/doi/pdf/10.1029/2010JC006547) doi: 10.1029/2010JC006547

Jacox, M. G., Edwards, C. A., Hazen, E. L., & Bograd, S. J. (2018). Coastal Upwelling Revisited:

Ekman, Bakun, and Improved Upwelling Indices for the U.S. West Coast. *Journal of Geophysical Research: Oceans*, *123*(10), 7332–7350. Retrieved 2020-07-07, from https://agupubs.onlinelibrary.wiley.com/doi/abs/10.1029/2018JC014187 (_eprint: https://agupubs.onlinelibrary.wiley.com/doi/pdf/10.1029/2018JC014187) doi: 10.1029/2018JC014187

Jacox, M. G., Hazen, E. L., & Bograd, S. J. (2016, June). Optimal Environmental Conditions and Anomalous Ecosystem Responses: Constraining Bottom-up Controls of Phytoplankton Biomass in the California Current System. *Scientific Reports*, *6*(1), 27612. Retrieved 2022-07-22, from https://www.nature.com/articles/srep27612 (Number: 1 Publisher: Nature Publishing Group) doi: 10.1038/srep27612

Jönsson, B. F., & Salisbury, J. E. (2016). Episodicity in phytoplankton dynamics in a coastal region. *Geophysical Research Letters*, *43*(11), 5821–5828.

Jorgensen, E. M., Hazen, E. L., Jacox, M. G., Pozo Buil, M., Schroeder, I., & Bograd, S. J. (2024). Physical and biogeochemical phenology of coastal upwelling in the california current system. *Geophysical Research Letters*, *51*(7), e2024GL108194. Retrieved from https://agupubs.onlinelibrary.wiley.com/doi/abs/10.1029/2024GL108194 (e2024GL108194 2024GL108194) doi: https://doi.org/10.1029/2024GL108194

Kämpf, J., & Chapman, P. (2016). *Upwelling systems of the world.* Springer.

Key, R. M., Kozyr, A., Sabine, C. L., Lee, K., Wanninkhof, R., Bullister, J. L., . . . Peng, T.-H. (2004). A global ocean carbon climatology: Results from Global Data Analysis Project (GLODAP). *Global Biogeochemical Cycles*, *18*(4). Retrieved 2022-10-28, from https://onlinelibrary.wiley.com/doi/abs/10.1029/2004GB002247 (_eprint: https://onlinelibrary.wiley.com/doi/pdf/10.1029/2004GB002247) doi: 10.1029/2004GB002247

Kwiatkowski, L., Aumont, O., & Bopp, L. (2019). Consistent trophic amplification of marine biomass declines under climate change. *Global Change Biology*, *25*(1), 218–229. Retrieved 2022-07-22, from https://onlinelibrary.wiley.com/doi/abs/10.1111/gcb.14468 (_eprint: https://onlinelibrary.wiley.com/doi/pdf/10.1111/gcb.14468) doi: 10.1111/gcb.14468

Lampe, R. H., Hernandez, G., Lin, Y. Y., & Marchetti, A. (2021). Representative diatom and coccolithophore species exhibit divergent responses throughout simulated upwelling cycles. *Msystems*, *6*(2), 10–1128.

Large, W. G., McWilliams, J. C., & Doney, S. C. (1994). Oceanic vertical mixing: A review and a

model with a nonlocal boundary layer parameterization. *Reviews of Geophysics*, *32*(4), 363–403. Retrieved 2021-11-22, from https://onlinelibrary.wiley.com/doi/abs/10.1029/94RG01872 (_eprint: https://onlinelibrary.wiley.com/doi/pdf/10.1029/94RG01872) doi: 10.1029/94RG01872

Largier, J. L. (2020). Upwelling Bays: How Coastal Upwelling Controls Circulation, Habitat, and Productivity in Bays. *Annual Review of Marine Science*, *12*(1), 415–447. Retrieved 2022-03-24, from https://doi.org/10.1146/annurev-marine-010419-011020 (_eprint: https://doi.org/10.1146/annurev-marine-010419-011020) doi: 10.1146/annurev-marine-010419-011020

Largier, J. L., Lawrence, C. A., Roughan, M., Kaplan, D. M., Dever, E. P., Dorman, C. E., . . . Koračin, D. (2006, December). WEST: A northern California study of the role of wind-driven transport in the productivity of coastal plankton communities. *Deep Sea Research Part II: Topical Studies in Oceanography*, *53*(25), 2833–2849. Retrieved 2022-09-28, from https://www.sciencedirect.com/science/article/pii/S0967064506002141 doi: 10.1016/j.dsr2.2006.08.018

Machu, E., Capet, X., Estrade, P. A., Ndoye, S., Brajard, J., Baurand, F., . . . Brehmer, P. (2019). First Evidence of Anoxia and Nitrogen Loss in the Southern Canary Upwelling System. *Geophysical Research Letters*, *46*(5), 2619–2627. Retrieved 2022-03-23, from https://onlinelibrary.wiley.com/doi/abs/10.1029/2018GL079622 (_eprint: https://onlinelibrary.wiley.com/doi/pdf/10.1029/2018GL079622) doi: 10.1029/2018GL079622

Marañón, E. (2015). Cell size as a key determinant of phytoplankton metabolism and community structure. *Annual review of marine science*, *7*, 241–264.

Menge, B. A., & Menge, D. N. (2013). Dynamics of coastal meta-ecosystems: the intermittent upwelling hypothesis and a test in rocky intertidal regions. *Ecological Monographs*, *83*(3), 283–310.

Messié, M., Ledesma, J., Kolber, D. D., Michisaki, R. P., Foley, D. G., & Chavez, F. P. (2009, December). Potential new production estimates in four eastern boundary upwelling ecosystems. *Progress in Oceanography*, *83*(1-4), 151–158. Retrieved 2022-12-05, from https://linkinghub.elsevier.com/retrieve/pii/S0079661109000731 doi: 10.1016/j.pocean.2009.07.018

Nagai, T., Gruber, N., Frenzel, H., Lachkar, Z., McWilliams, J. C., & Plattner, G.-K. (2015). Dominant role of eddies and filaments in the offshore transport of carbon and nutrients in the California

Current System. *Journal of Geophysical Research: Oceans*, *120*(8), 5318–5341. Retrieved 2022-07-22, from https://onlinelibrary.wiley.com/doi/abs/10.1002/2015JC010889 (_eprint: https://onlinelibrary.wiley.com/doi/pdf/10.1002/2015JC010889) doi: 10.1002/2015JC010889

NASA. (2014). *NASA Goddard Space Flight Center, Ocean Ecology Laboratory, Ocean Biology Processing Group. Moderate-resolution Imaging Spectroradiometer (MODIS) Aqua 11μm Day/Night Sea Surface Temperature Data. NASA OB.DAAC, Greenbelt, MD, USA*. Retrieved from https://oceancolor.gsfc.nasa.gov/data/10.5067/AQUA/MODIS/L3M/SST/2014/ doi: data/10.5067/AQUA/MODIS/L3M/SST/2014

Ndoye, S., Capet, X., Estrade, P., Sow, B., Machu, E., Brochier, T., ... Brehmer, P. (2017). Dynamics of a "low-enrichment high-retention" upwelling center over the southern Senegal shelf. *Geophysical Research Letters*, *44*(10), 5034–5043. Retrieved 2021-11-22, from https://onlinelibrary.wiley.com/doi/abs/10.1002/2017GL072789 (_eprint: https://onlinelibrary.wiley.com/doi/pdf/10.1002/2017GL072789) doi: 10.1002/2017GL072789

Pfaff, M. C., Branch, G. M., Fisher, J. L., Hoffmann, V., Ellis, A. G., & Largier, J. L. (2015). Delivery of marine larvae to shore requires multiple sequential transport mechanisms. *Ecology*, *96*(5), 1399–1410.

Philander, S., & Yoon, J. (1982). Eastern boundary currents and coastal upwelling. *Journal of Physical Oceanography*, *12*(8), 862–879.

Pietri, A., Colas, F., Mogollon, R., Tam, J., & Gutierrez, D. (2021). Marine heatwaves in the humboldt current system: from 5-day localized warming to year-long el niños. *Scientific Reports*, *11*(1), 21172.

Pringle, J. M. (2002, November). Enhancement of Wind-Driven Upwelling and Downwelling by Alongshore Bathymetric Variability. *Journal of Physical Oceanography*, *32*(11), 3101–3112. Retrieved 2021-11-22, from https://journals.ametsoc.org/view/journals/phoc/32/11/1520-0485_2002_032_3101_eowdua_2.0.co_2.xml (Publisher: American Meteorological Society Section: Journal of Physical Oceanography) doi: 10.1175/1520-0485(2002)032⟨3101:EOWDUA⟩2.0.CO;2

Renault, L., Deutsch, C., McWilliams, J. C., Frenzel, H., Liang, J.-H., & Colas, F. (2016, July). Partial decoupling of primary productivity from upwelling in the California Current system. *Nature Geoscience*, *9*(7), 505–508. Retrieved 2022-09-28, from

https://www.nature.com/articles/ngeo2722 (Number: 7 Publisher: Nature Publishing Group) doi: 10.1038/ngeo2722

Risien, C. M., & Chelton, D. B. (2008, November). A Global Climatology of Surface Wind and Wind Stress Fields from Eight Years of QuikSCAT Scatterometer Data. *Journal of Physical Oceanography*, *38*(11), 2379–2413. Retrieved 2021-11-22, from https://journals.ametsoc.org/view/journals/phoc/38/11/2008jpo3881.1.xml (Publisher: American Meteorological Society Section: Journal of Physical Oceanography) doi: 10.1175/2008JPO3881.1

Send, U., Beardsley, R. C., & Winant, C. D. (1987). Relaxation from upwelling in the Coastal Ocean Dynamics Experiment. *Journal of Geophysical Research: Oceans*, *92*(C2), 1683–1698. Retrieved 2021-11-22, from https://onlinelibrary.wiley.com/doi/abs/10.1029/JC092iC02p01683 (_eprint: https://onlinelibrary.wiley.com/doi/pdf/10.1029/JC092iC02p01683) doi: 10.1029/JC092iC02p01683

Shchepetkin, A. F., & McWilliams, J. C. (2005, January). The regional oceanic modeling system (ROMS): a split-explicit, free-surface, topography-following-coordinate oceanic model. *Ocean Modelling*, *9*(4), 347–404. Retrieved 2022-10-12, from https://www.sciencedirect.com/science/article/pii/S1463500304000484 doi: 10.1016/j.ocemod.2004.08.002

Shchepetkin, A. F., & McWilliams, J. C. (2009, December). Correction and commentary for "Ocean forecasting in terrain-following coordinates: Formulation and skill assessment of the regional ocean modeling system" by Haidvogel et al., J. Comp. Phys. 227, pp. 3595–3624. *Journal of Computational Physics*, *228*(24), 8985–9000. Retrieved 2021-11-22, from https://www.sciencedirect.com/science/article/pii/S0021999109004872 doi: 10.1016/j.jcp.2009.09.002

Sommer, U., Stibor, H., Katechakis, A., Sommer, F., & Hansen, T. (2002). Pelagic food web configurations at different levels of nutrient richness and their implications for the ratio fish production: primary production. In *Sustainable increase of marine harvesting: Fundamental mechanisms and new concepts: Proceedings of the 1st maricult conference held in trondheim, norway, 25–28 june 2000* (pp. 11–20).

Spitz, Y. H., Allen, J. S., & Gan, J. (2005). Modeling of ecosystem processes on the Oregon shelf

during the 2001 summer upwelling. *Journal of Geophysical Research: Oceans*, *110*(C10). Retrieved 2022-10-10, from https://onlinelibrary.wiley.com/doi/abs/10.1029/2005JC002870 (_eprint: https://onlinelibrary.wiley.com/doi/pdf/10.1029/2005JC002870) doi: 10.1029/2005JC002870

Steele, J. H., & Henderson, E. W. (1992). The role of predation in plankton models. *Journal of Plankton Research*, *14*(1), 157–172.

Stukel, M. R., Aluwihare, L. I., Barbeau, K. A., Chekalyuk, A. M., Goericke, R., Miller, A. J., ... Landry, M. R. (2017, February). Mesoscale ocean fronts enhance carbon export due to gravitational sinking and subduction. *Proceedings of the National Academy of Sciences*, *114*(6), 1252–1257. Retrieved 2020-07-07, from https://www.pnas.org/content/114/6/1252 (Publisher: National Academy of Sciences Section: Physical Sciences) doi: 10.1073/pnas.1609435114

Tall, A. W., Machu, E., Echevin, V., Capet, X., Pietri, A., Corréa, K., ... Lazar, A. (2021). Variability of Dissolved Oxygen in the Bottom Layer of the Southern Senegalese Shelf. *Journal of Geophysical Research: Oceans*, *126*(5), e2020JC016854. Retrieved 2021-11-22, from https://onlinelibrary.wiley.com/doi/abs/10.1029/2020JC016854 (_eprint: https://onlinelibrary.wiley.com/doi/pdf/10.1029/2020JC016854) doi: 10.1029/2020JC016854

Tegen, I., & Fung, I. (1994). Modeling of mineral dust in the atmosphere: Sources, transport, and optical thickness. *Journal of Geophysical Research: Atmospheres*, *99*(D11), 22897–22914. Retrieved 2022-10-28, from https://onlinelibrary.wiley.com/doi/abs/10.1029/94JD01928 (_eprint: https://onlinelibrary.wiley.com/doi/pdf/10.1029/94JD01928) doi: 10.1029/94JD01928

Thomsen, S., Capet, X., & Echevin, V. (2021, November). Competition between Baroclinic Instability and Ekman Transport under Varying Buoyancy Forcings in Upwelling Systems: An Idealized Analog to the Southern Ocean. *Journal of Physical Oceanography*, *51*(11), 3347–3364. Retrieved 2022-03-24, from https://journals.ametsoc.org/view/journals/phoc/51/11/JPO-D-20-0294.1.xml (Publisher: American Meteorological Society Section: Journal of Physical Oceanography) doi: 10.1175/JPO-D-20-0294.1

Vander Woude, A. J., Largier, J. L., & Kudela, R. M. (2006). Nearshore retention of upwelled waters north and south of point reyes (northern california)—patterns of surface temperature and chlorophyll observed in coop west. *Deep Sea Research Part II: Topical Studies in Oceanography*,

53(25-26), 2985–2998.

Wang, Q., & Mu, M. (2014). Responses of the ocean planktonic ecosystem to finite-amplitude perturbations. *Journal of Geophysical Research: Oceans*, *119*(12), 8454–8471.

Ward, B. A., Dutkiewicz, S., & Follows, M. J. (2014). Modelling spatial and temporal patterns in size-structured marine plankton communities: top–down and bottom–up controls. *Journal of Plankton Research*, *36*(1), 31–47.

Wilkerson, F. P., Lassiter, A. M., Dugdale, R. C., Marchi, A., & Hogue, V. E. (2006, December). The phytoplankton bloom response to wind events and upwelled nutrients during the CoOP WEST study. *Deep Sea Research Part II: Topical Studies in Oceanography*, *53*(25), 3023–3048. Retrieved 2022-04-01, from https://www.sciencedirect.com/science/article/pii/S0967064506002232 doi: 10.1016/j.dsr2.2006.07.007

Worley, S. J., Woodruff, S. D., Reynolds, R. W., Lubker, S. J., & Lott, N. (2005). ICOADS release 2.1 data and products. *International Journal of Climatology*, *25*(7), 823–842. Retrieved 2021-11-22, from https://onlinelibrary.wiley.com/doi/abs/10.1002/joc.1166 (_eprint: https://onlinelibrary.wiley.com/doi/pdf/10.1002/joc.1166) doi: 10.1002/joc.1166

Yokomizo, H., Botsford, L. W., Holland, M. D., Lawrence, C. A., & Hastings, A. (2010). Optimal wind patterns for biological production in shelf ecosystems driven by coastal upwelling. *Theoretical Ecology*, *3*, 53–63.